Molecular Crystals and Liquid Crystals
Publication details, including instructions for authors and subscription information:
http://www.tandfonline.com/loi/gmcl16

Heat Capacity and Phase Transitions of Thiourea-Ferrocene Channel Inclusion Compound

Michio Sorai [a] , Kouji Ogasahara [a b] & Hiroshi Suga [a]
[a] Department of Chemistry and Chemical Termodynamics Laboratory, Faculty of Science, Osaka University, toyonaka, Osaka, 560, Japan
[b] Integrated Circuit Section, Sharp Corporation, Tenri, Nara, 632, Japan
Version of record first published: 20 Apr 2011.

To cite this article: Michio Sorai , Kouji Ogasahara & Hiroshi Suga (1981): Heat Capacity and Phase Transitions of Thiourea-Ferrocene Channel Inclusion Compound, Molecular Crystals and Liquid Crystals, 73:3-4, 231-254

To link to this article: http://dx.doi.org/10.1080/00268948108072337

Mol. Cryst. Liq. Cryst., 1981, Vol. 73, pp. 231–254
0026-8941/81/7304–0231$06.50/0

Printed in the United States of America

Heat Capacity and Phase Transitions of Thiourea-Ferrocene Channel Inclusion Compound†

MICHIO SORAI, KOUJI OGASAHARA‡ and HIROSHI SUGA

Department of Chemistry and Chemical Thermodynamics Laboratory, Faculty of Science, Osaka University, Toyonaka, Osaka 560, Japan

(*Received February 24, 1981*)

The heat capacity of a 3:1 thiourea-ferrocene channel inclusion compound has been measured with an adiabatic-type calorimeter between 13 and 280 K. Five phase transitions were found at 147.2 (T_{C1}), 159.79 (T_{C2}), 171.4 (T_{C3}), 185.5 (T_{C4}) and 220 K (T_{C5}). The enthalpy and entropy associated with these transitions have been determined. The two lowest-temperature transitions are responsible for an order-disorder-type of reorientation of the molecular axis of ferrocene in the thiourea host lattice. This reorientational disordering was proved to proceed in two steps; in the first stage the reorientational motion is excited within the channel plane in a group of, say, three ferrocene molecules as a unit keeping the short-range order while in the second stage this restriction is lifted and the jump process between the channel plane and the channel axis is allowed. The remaining three phase transitions with small entropy change have been attributed to unknown but intrinsic characters of the present clathrate. The dielectric constant measurements revealed no ferroelectric nature. The infrared and Raman spectra have also been recorded. Comparison of the transition mechanisms between solid ferrocene and the present clathrate has been made.

1 INTRODUCTION

As in the case of urea, thiourea is known to form channel inclusion compounds.[1,2] Owing to the larger channel diameter (0.61 nm) of the thiourea host-lattice than the 0.525 nm of urea, the former can include branched-chain

† Contribution No. 15 from Chemical Thermodynamics Laboratory. A part of this paper was presented at the 13th Annual Meeting of the Society of Calorimetry and Thermal Analysis, Japan, Tokyo (1977).

‡ Present address: Integrated Circuit Section, Sharp Corporation, Tenri, Nara 632, Japan.

paraffins or cycloalkanes as well. In 1974 Clement, Claude and Mazieres[3] reported new clathration of ferrocene, $Fe(C_5H_5)_2$, in thiourea host-lattice channels. The ratio of thiourea to ferrocene molecules is 3.0, a value equal to that found for the cyclohexane clathrate. The crystal structure[3,4] has the same rhombohedral unit cell ($R\bar{3}c$ with $Z = 6$) as that of the known thiourea clathrates.[5] When referred to hexagonal axes, the measured parameters[3] are $a = 1.640$ nm (1.6360 nm)[4] and $c = 1.250$ nm (1.2395 nm)[4], thus showing an appreciable expansion of the host-lattice in the a-direction with respect to the cyclohexane clathrate[5] where $a = 1.58$ nm and $c = 1.25$ nm.

Clement *et al.*[3] found a first-order phase transition at 162 K in the thiourea-ferrocene inclusion compound by differential thermal analysis. Gibb[6] studied in detail the temperature dependence of the ^{57}Fe Mössbauer effect of this compound and found an interesting anisotropic relaxation of the electric field gradient tensor across the phase transition point. He attributed this relaxation phenomenon to anisotropic reorientation of the ferrocene molecules in the channels of the clathrate lattice.

We were much interested in the mechanism of this phase transition in comparison with those of pure ferrocene crystals. Recently we[7-9] found a new low-temperature phase in solid ferrocene which is stable below 242 K and pointed out that the well-known λ-type phase transition at 163.9 K reported by Edwards *et al.*[10,11] is a transition between metastable phases. This finding was crystallographically confirmed by Berar *et al.*[12] Although detailed interpretations on molecular basis have not been given, the transition mechanism was revealed to be quite different between the λ-type and the new phase transitions.[7-9,12]

In the case of thiourea-ferrocene clathrate, each ferrocene molecule is trapped in a potential cage formed by the thiourea host-lattice and thus the intermolecular interaction between the guest molecules, ferrocene, seems to be indirect and weak. Moreover, the ferrocene molecule has a rather globular form and is electrically non-polar. Hence for the present case, one cannot expect transition mechanisms such as (i) the cooperative coupling between deformation of the host-channels and rotational motion of the guest molecules encountered in the thiourea adduct with 2,3-dimethyl-butadiene[13] or urea adducts with *n*-paraffins[14] and (ii) the orientational order-disorder mechanism coupled with strong electric dipole moments of HCN and CH_3OH in quinol clathrates.[15,16]

The purpose of the present paper is to throw light upon the mechanism of this new type of phase transition from a thermodynamic point of view, especially in comparison with those of pure ferrocene crystal. The main tool adopted here is adiabatic calorimetry between 13 and 280 K. Auxiliary measurements of infrared and Raman spectra and dielectric constant have also been made as a function of temperature.

2 EXPERIMENTAL

Sample preparation

The thiourea-ferrocene inclusion compound was prepared by the method of Clement *et al.*[3] except that we used ethanol instead of methanol as the solvent. In the case of methanol, we could not avoid admixture of a trace of pure ferrocene crystallites in the products whereas no such undesirable problem occurred for ethanol. The orange needle crystals of thiourea-ferrocene clathrate thus obtained were washed three times with cold ethanol, dried in a stream of dry-nitrogen gas for 43 h and finally dried in a vacuum for 20 min. It should be remarked that long evacuation of the compound leads to a partial escape of ferrocene molecules from the thiourea channel lattice even at room temperature. *Anal.* Calcd. for $Fe(C_5H_5)_2 \cdot 3(NH_2)_2CS$: C, 37.68%; H, 5.35%; N, 20.28%; Fe, 13.48%. Found: C, 37.39%; H, 5.35%; N, 20.25%; Fe, 13.39%.

In order to determine the stoichiometry of the clathrate, 2.2321 g of the sample was heated up to 60°C in a vacuum for 40 h. Under this condition, only the guest molecules, ferrocene, were sublimated and a white residue of thiourea remained, the mass of which was 1.2301 g. Based on this gravimetric analysis, the molar ratio of thiourea to ferrocene was determined to be 3.0005:1, indicating that the ideal stoichiometry of 3:1 has been established for the present sample.

Heat capacity measurements

The heat capacities were measured between 13 and 280 K with an adiabatic-type calorimeter.[17] A calorimeter cell made of gold-plated copper[9] contained 16.4843 g (≙ 0.0397803 mol) of the specimen and a small amount of helium gas to aid the heat transfer. A platinum resistance thermometer (Leeds & Northrup Co., Ltd.) used in this experiment has been calibrated based on the IPTS-68 temperature scale.

Infrared and Raman spectroscopy

Infrared spectra in the range 4000–400 cm^{-1} were recorded for Nujol mulls and KBr disc with an Infrared Spectrophotometer Model DS-402G (Japan Spectroscopic Co., Ltd.) and far infrared spectra in the range 400–30 cm^{-1} with a Far Infrared Spectrophotometer Model FIS-3 (Hitachi, Ltd.) between 100 and 300 K. To examine closely the temperature dependence of the spectra in the range 520–460 cm^{-1} and 200–100 cm^{-1}, the spectra were recorded with a wavenumber expansion method, ×4 and ×2, respectively. Temperature was measured by a copper-constantan thermocouple and controlled within ±1 K.

Raman spectra in the range 4000–30 cm^{-1} were recorded for KBr disc with a Laser Raman Spectrophotometer Model R750 (Japan Spectroscopic Co.,

Ltd.) using the 514.5 nm line from an argon-ion source for excitation as a function of temperature.

Dielectric measurements

The dielectric constant (relative permittivity) of the present clathrate was measured at 1 kHz with a transformer bridge (General Radio, Type 1620 Capacitance Measuring System) in the range 80–280 K. The cryostat and the measuring assembly were described previously.[18] As it was difficult to obtain a plate-like single crystal of this compound, the needle crystals were powdered in an agate mortar and pressed at 25–35 kg cm^{-2} under evacuation. The dimensions of the pellets prepared for the probe were 13.08 mm in diameter and 0.901 and 1.184 mm in thickness. Conducting silver paint was applied to both faces of the pellets.

3 RESULTS

Heat capacity and related quantities

The results of the calorimetric measurements were evaluated in terms of C_p, the molar heat capacity, based on a relative molecular mass of 414.384 for $Fe(C_5H_5)_2 \cdot 3(NH_2)_2CS$. The experimental data are listed in Table I and plotted in Figure 1.

TABLE I

Molar heat capacity of $Fe(C_5H_5)_2 \cdot 3(NH_2)_2CS$; relative molecular mass being 414.384

T_{av} / K	C_p / J K^{-1} mol^{-1}	T_{av} / K	C_p / J K^{-1} mol^{-1}	T_{av} / K	C_p / J K^{-1} mol^{-1}
85.69	187.03	183.99	330.24	69.27	162.31
88.01	190.12	184.85	334.27	71.15	165.35
90.36	193.42	185.71	333.70	72.98	168.32
92.77	196.57	186.57	330.22	74.91	171.31
95.25	199.88	187.43	331.09	76.93	174.48
97.67	203.25	188.29	332.24	78.91	177.35
100.05	206.58	189.14	333.10	80.96	180.32
102.39	209.81	190.84	335.10	83.18	183.54
104.69	212.77	193.38	338.54		
107.11	216.03	195.90	341.86	122.51	236.87
109.64	219.41	198.40	345.28	125.07	240.37
112.12	222.69	200.88	348.81		
114.58	225.89	203.35	352.60	13.23	12.88
116.99	229.25	205.80	356.15	14.21	15.52
119.38	232.49	208.34	360.02	15.19	18.20
121.73	235.58	210.96	364.40	16.10	20.56

TABLE I (*continued*)

Molar heat capacity of $Fe(C_5H_5)_2 \cdot 3(NH_2)_2CS$; relative molecular mass being 414.384

T_{av} / K	C_p / J K^{-1} mol^{-1}	T_{av} / K	C_p / J K^{-1} mol^{-1}	T_{av} / K	C_p / J K^{-1} mol^{-1}
121.22	235.06	212.79	367.54	17.05	23.37
123.80	238.66	213.83	369.37	19.14	29.63
126.34	242.38	214.87	371.04	20.15	32.82
128.86	245.88	215.91	372.73	21.25	36.27
131.34	249.49	216.94	374.65	22.40	39.90
133.79	253.27	217.97	376.70	23.55	43.62
136.22	257.07	218.99	378.20	24.71	47.43
138.62	260.76	220.02	379.50	25.91	51.40
140.99	264.62	221.04	380.30	27.18	55.61
143.34	268.71	222.06	378.41	28.52	60.09
144.76	270.49	223.08	378.87	29.94	64.67
145.51	276.17	224.10	379.70	31.40	69.46
146.49	297.83	225.12	381.25	32.90	74.40
147.45	315.47	226.14	381.86	34.42	79.30
148.40	295.38	227.15	383.72	35.94	84.23
149.37	293.43	229.17	386.28	37.46	89.09
150.34	295.96	232.18	390.29	38.99	93.46
151.30	297.16	235.17	394.13	40.53	98.28
152.50	298.79	238.15	398.03	42.07	102.51
153.93	302.78	241.11	402.16	43.63	106.74
155.35	307.89	243.17	404.56	45.15	110.94
156.75	313.21	244.91	407.51	46.59	114.76
158.14	319.34	247.80	411.93		
159.28	363.50	251.24	416.93	83.26	183.57
159.79	4068.0	255.01	422.29	85.62	186.96
160.15	869.45	259.11	428.27		
160.73	750.55	263.17	433.96	124.47	239.65
161.24	397.38	267.21	439.27		
161.68	311.63	271.22	445.07	144.05	270.05
162.15	298.90	275.19	450.78	145.13	273.98
162.62	299.20	279.13	456.35	146.01	286.25
163.09	299.10			146.99	320.27
163.79	300.49	46.88	115.37	147.92	290.77
164.72	300.98	48.02	118.37	148.91	293.26
165.64	302.35	49.13	121.29		
166.80	304.16	50.20	123.99	218.48	377.37
168.18	306.25	51.23	126.51	219.50	378.73
169.56	308.78	52.42	129.21		
170.70	313.33	53.80	132.28	220.52	380.46
171.61	315.12	55.33	135.86	221.55	379.88
172.52	312.60	56.95	139.27	222.57	378.57
173.43	313.71	58.51	142.55		
174.34	314.93	60.01	145.46		
175.24	316.39	61.49	148.27		
176.68	318.30	62.95	151.03		
178.67	320.84	64.45	153.82		
180.64	323.92	65.98	156.68		
182.60	327.62	67.53	159.38		

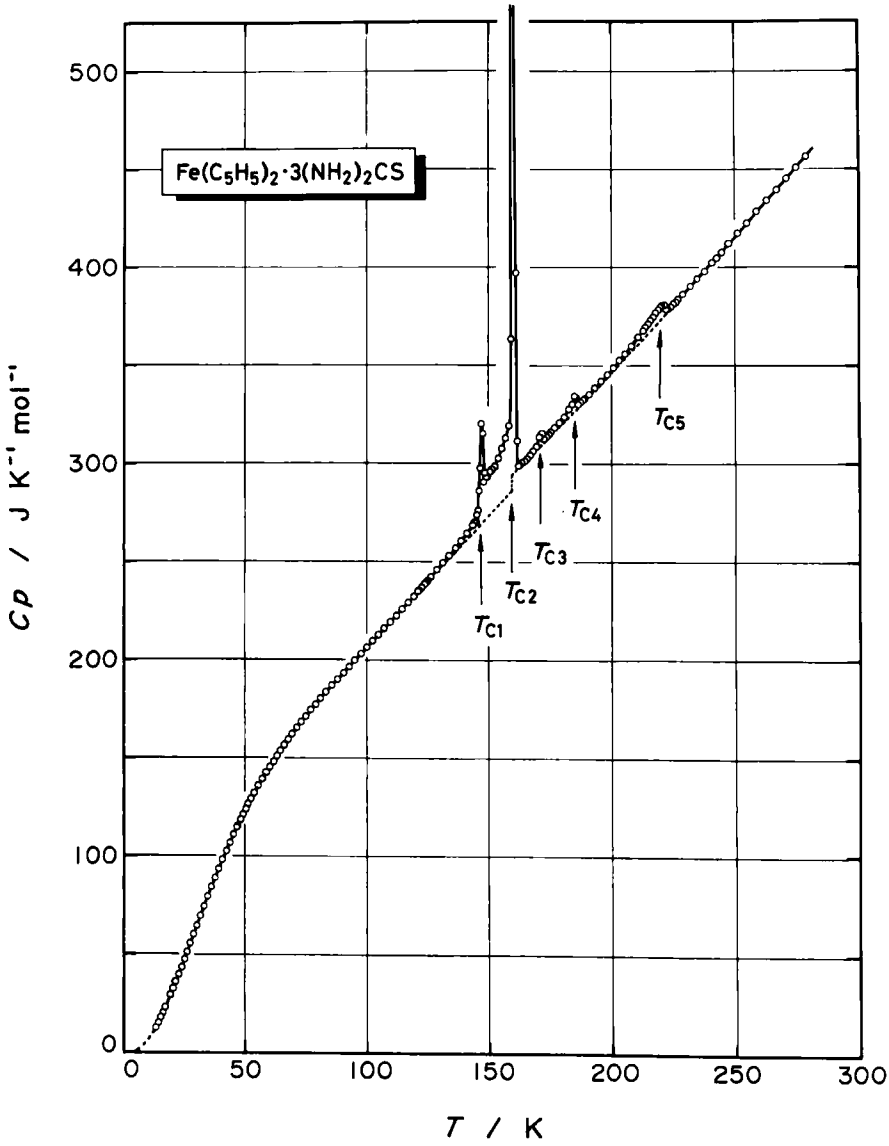

FIGURE 1 Molar heat capacity of $Fe(C_5H_5)_2 \cdot 3(NH_2)_2CS$. Broken lines represent the "normal" heat capacities.

Five well-defined heat capacity anomalies were found at 147.2, 159.79, 171.4, 185.5 and 220 K. As will be discussed below, these anomalies are associated with phase transitions. We shall, therefore, designate these transition points as $T_{Cn}(n = 1, 2, 3, 4 \text{ and } 5)$ in order of increasing temperature. The crystalline phases bounded by T_{Cn} will be named as Phases I, II, . . ., VI in de-

scending direction of temperature: *e.g.*, the room-temperature phase corresponds to Phase I and the lowest temperature phase below T_{C1} is Phase VI.

The phase transition at T_{C2} characterized by the largest transition enthalpy among the five showed an undercooling effect; indicating that this phase transition is obviously of first-order. The time interval required for thermal equilibration after an energy input was usually within 10 min even in the vicinity of T_{C3}, T_{C4} and T_{C5}; suggesting that these three phase transitions are of second-order. However, in the range 146–162 K including T_{C1} and T_{C2}, endothermic drift of temperature lasted from tens of minutes to several hours depending on the temperature region. The long temperature drifts followed exponential decays, from which we could estimate the equilibrium temperatures. Although a long equilibration time is generally encountered for a first-order phase transition, it was difficult to judge whether or not the transition at T_{C1} could be classified as a first-order transition.

The thermodynamic functions of the thiourea-ferrocene inclusion compound were calculated from the heat-capacity data and the calorimetric enthalpy measurements across the respective phase transitions. Table II contains a listing of values for the heat capacity, C_p°, the entropy, S°, the enthalpy function, $(H^\circ - H_0^\circ)/T$, and the Gibbs energy function, $-(G^\circ - H_0^\circ)/T$, at selected temperatures.

It should be remarked that Clement *et al.*[3] found only a first-order phase transition at 162 K by differential thermal analysis (DTA). It is obvious that their finding corresponds to the strongest transition at T_{C2} of the present work.

Dielectric constant

The dielectric constant measurements were made for two pellet-probes with thicknesses of 0.901 and 1.184 mm. The thick pellet, however, gave no reproducible results for temperature cycling. This was caused by cracks parallel to the pellet-face. In the case of the thin pellet, the cracking effect was avoided and the dielectric constants coincided at a given temperature within ±0.2%.

Figure 2 shows the dielectric constants of the present clathrate with the pellet thickness of 0.901 mm determined during heating. The dielectric constant (ϵ_r: relative permittivity) gradually increased with increasing temperature. After passing T_{C1} the gradient, $d\epsilon_r/dT$, became steeper and at T_{C2} a discontinuity occurred from 3.51 to 3.59. On further heating, ϵ_r increased monotonically without showing any anomalies at T_{C3} and T_{C4}, though a recognizable small jump beyond the present experimental errors was detected at T_{C5} (see the insert of Figure 2).

Since the temperature dependence of ϵ_r has been drawn on an enlarged scale in Figure 2, the change in the dielectric constant at T_{C2} seems to be drastic. However, the absolute value of ϵ_r itself is very small and comparable with those found for solids consisting of non-polar molecules. Therefore, ferroelec-

TABLE II

Standard thermodynamic functions for $Fe(C_5H_5)_2 \cdot 3(NH_2)_2CS$

T	C_p°	S°	$(H^\circ - H_0^\circ)/T$	$-(G^\circ - H_0^\circ)/T$
K	J K^{-1} mol^{-1}	J K^{-1} mol^{-1}	J K^{-1} mol^{-1}	J K^{-1} mol^{-1}
10	(6.87)	(2.56)	(1.89)	(0.67)
20	32.36	14.21	10.07	4.13
30	64.88	33.42	22.87	10.54
40	96.63	52.82	37.42	15.41
50	123.49	81.03	52.01	29.02
60	145.43	105.56	65.82	39.74
70	163.49	129.38	78.52	50.86
80	178.94	152.24	90.13	62.11
90	192.91	174.13	100.78	73.35
100	206.51	195.15	110.67	84.49
110	219.89	215.47	119.99	95.47
120	233.31	235.17	128.87	106.30
130	247.54	254.89	137.91	116.98
140	263.01	273.79	146.28	127.51
150	295.07 (transition)	293.18	155.28	137.89
170	310.53	339.38	180.46	158.92
180	322.92	357.48	188.03	169.45
190	334.11	375.32	195.50	179.82
200	347.56	392.79	202.76	190.03
210	362.79	410.11	210.01	200.10
220	379.48	427.38	217.34	210.04
230	387.39	444.35	224.49	219.86
240	400.62	461.11	231.55	229.56
250	415.13	477.75	238.60	239.16
260	429.52	494.32	245.67	248.65
270	443.30	510.78	252.73	258.06
280	457.60	527.16	259.79	267.37
273.15	447.84	516.05	254.95	261.10

tricity having been found for pure thiourea crystal[19,20] cannot be expected for the thiourea-ferrocene clathrate. In the present dielectric measuring system, a geometrical capacitance of the electrode is directly influenced by thermal expansion of a specimen. Thus the gradual slope of ϵ_r below T_{C1} and above T_{C2} can be attributed to thermal expansion of the specimen due to anharmonic lattice vibrations, whereas the discontinuities at T_{C2} and T_{C5} might arise from different molar volumes below and above the respective transition temperatures. If this is the case, we can estimate a volume change associated with the transition at T_{C2} to be about 7%. As shown in Figure 2, the change in ϵ_r between T_{C1} and T_{C2} is rather large. If this region is included in the calculation, the net volume change across T_{C1} and T_{C2} amounts to 10%.

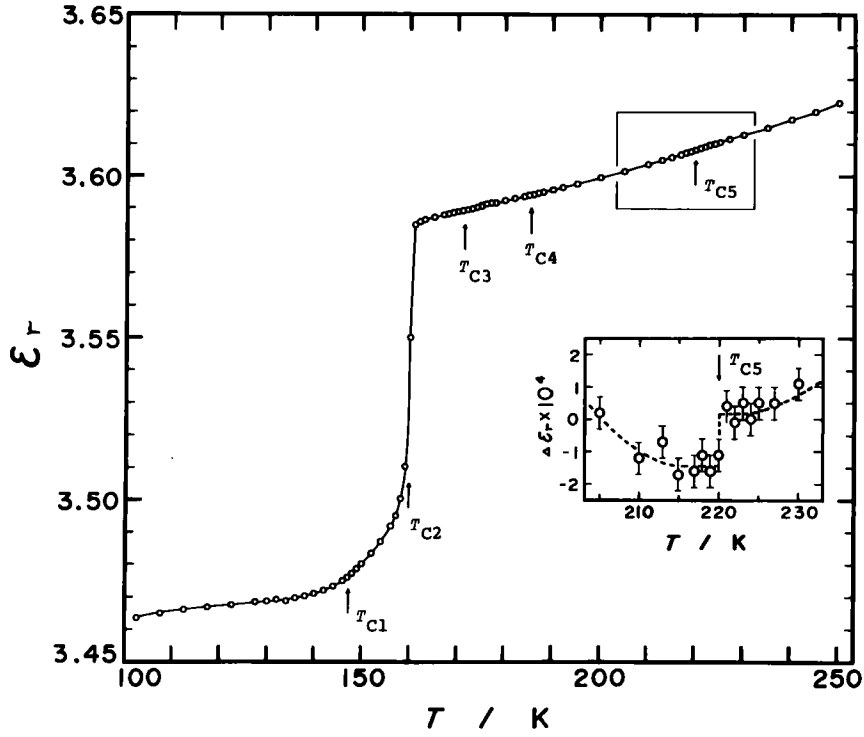

FIGURE 2 The dielectric constant of $Fe(C_5H_5)_2 \cdot 3(NH_2)_2CS$. The temperature dependence around T_{C5} is enlarged in the insert.

Infrared and Raman spectra

The gross aspect of the infrared and Raman spectra of the thiourea-ferrocene inclusion compound was simple superposition of the spectra of pure ferrocene[21] and thiourea crystals,[22-24] though the crystal structures are different between the pure components and the clathrate. The interesting wavenumber regions in relation to the phase transitions are those which include the metal-ring skeletal modes of ferrocene molecule. Among the six skeletal modes of ferrocene ($A_{1g} + E_{1g} + A_{1u} + A_{2u} + 2E_{1u}$), the symmetric metal-ring stretching $\nu_4(A_{1g})$ and the symmetric ring tilt $\nu_{16}(E_{1g})$ modes are Raman active, here the normal mode number is labelled according to that of the pure ferrocene crystal.[21] As shown in Figure 3, the ν_4 mode splits into a doublet at 323/313 cm^{-1} whereas the ν_{16} mode remained a singlet at 388 cm^{-1}. This feature is analogous to that of the monoclinic and triclinic phases of solid ferrocene. In the new low-temperature phase of ferrocene with orthorhombic system, the ν_{16} mode splits into a doublet and the ν_4 mode becomes a singlet.[8] It is therefore

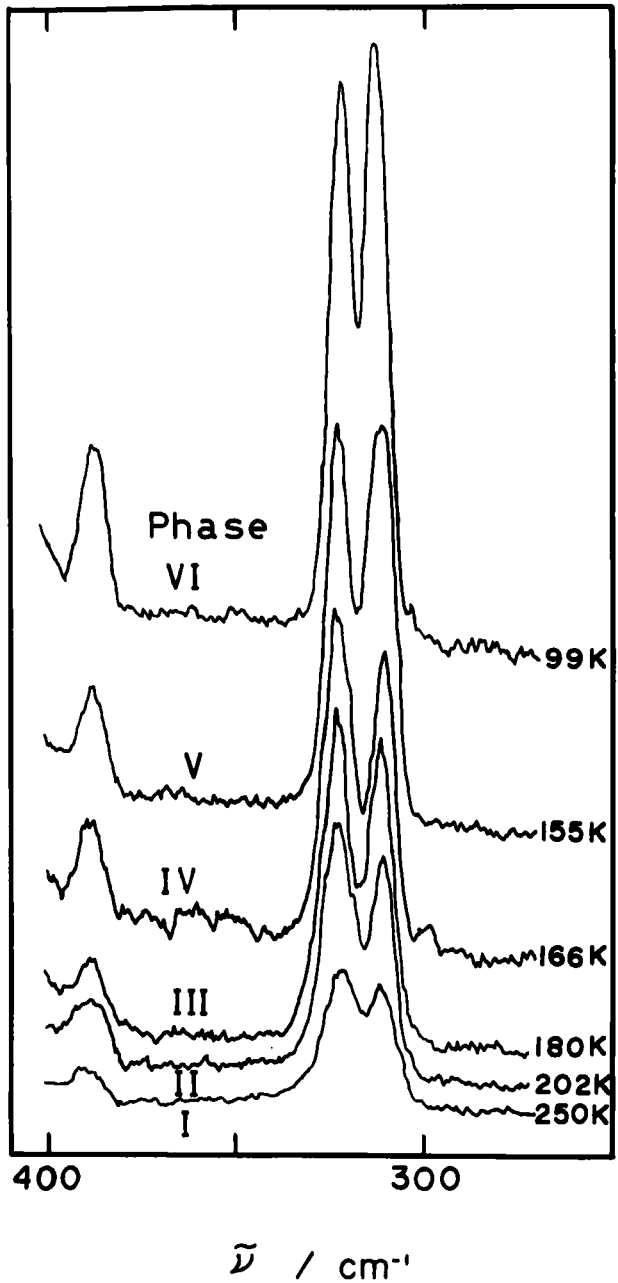

FIGURE 3 Raman spectra of $Fe(C_5H_5)_2 \cdot 3(NH_2)_2CS$ in the range 400–275 cm^{-1}.

concluded that the site symmetry of the potential cage, in which the ferrocene molecules of the clathrate are trapped, has a resemblance to that of the monoclinic or triclinic phases rather than the orthorhombic phase of pure ferrocene crystal.

The metal-ring torsional $\nu_6(A_{1u})$ mode is inactive for both infrared and Raman spectra, while the ring-metal-ring bending $\nu_{22}(E_{1u})$ mode is known to appear in the infrared spectrum around 180 cm^{-1}. Figure 4 illustrates the infrared spectra in the range 210–110 cm^{-1}. Although in the case of solid ferro-

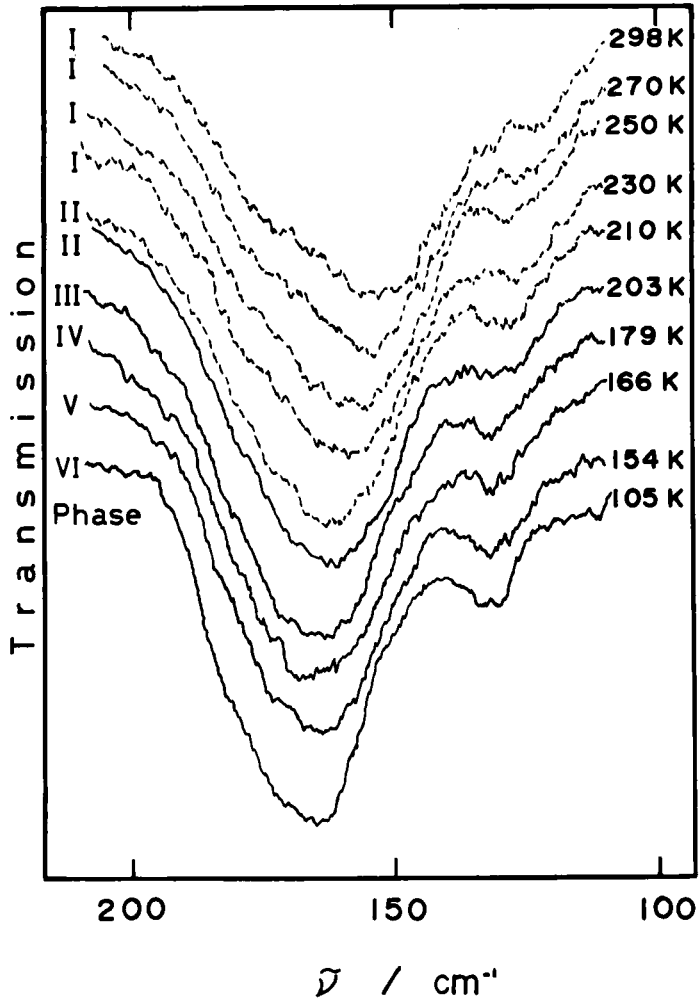

FIGURE 4 Infrared spectra of $Fe(C_5H_5)_2 \cdot 3(NH_2)_2CS$ in the range 210–110 cm^{-1} recorded for Nujol mulls.

cene the ν_{22} mode is well resolved into a triplet at 174/181/188 cm^{-1} at low temperatures,[25] the spectrum of the thiourea-ferrocene clathrate collapsed into a broad band. The apparent center of this band showed a rather large shift from 165 cm^{-1} at 105 K to 155 cm^{-1} at 298 K. A small band between 130–125 cm^{-1} has not been assigned.

The remaining two skeletal modes of ferrocene, the antisymmetric ring tilt $\nu_{21}(E_{1u})$ and the antisymmetric metal-ring stretching $\nu_{11}(A_{2u})$ modes, appear at 492 and 478 cm^{-1}, respectively.[21] Figure 5 shows the infrared spectra recorded for Nujol mulls of the clathrate in the range 520–460 cm^{-1}. In contrast to the case of solid ferrocene, the present spectrum contained two extra bands. One of them may arise from the NCN bending mode of the thiourea molecule.[22] In order to examine the temperature dependence of the position and intensity of the constituent bands, each spectrum was resolved into the component bands with the Gaussian form by a Curve Resolver (DuPont, Model 310). Two representative resolved-spectra are illustrated in Figure 6. To improve the base line, we had to record the spectra by using a KBr disc instead of Nujol mulls. In this case, however, an extra band appeared around 510 cm^{-1}. This band seems to be caused by the thiourea-KBr complex,[22] which was formed during preparation of the disc-probe. The two strong bands-1 and 3 may correspond to the $\nu_{11}(A_{2u})$ and $\nu_{21}(E_{1u})$ modes of solid ferrocene, while the strongest band-4 can be assigned to the NCN bending mode of the thiourea molecule because pure thiourea shows a very strong band due to this mode[22] at 486 cm^{-1} and also because the thiourea molecules in the clathrates are known to have the same shape as in pure thiourea crystals.[5] The increase in wavenumber from 486 cm^{-1} to the 508–514 cm^{-1} for the present clathrate may have resulted from the stronger hydrogen-bonding in the channel lattice compared with pure thiourea crystal. Assignment of the band-2 is open to question. As shown in Figure 6, shift of the position of the respective bands with temperature was very small while a change in the intensity was remarkable. No drastic change, however, could be detected at any phase transition points.

4 ENTHALPY AND ENTROPY OF PHASE TRANSITION

To separate the excess heat capacities due to the phase transitions from the experimental values, we must estimate appropriate "normal" heat capacities. As pointed out in Section 3, the phase transition at T_{C2} is of first-order and involves a volume change. Hence the normal heat capacity is expected to bring about a discontinuity at T_{C2}. The normal heat capacity below T_{C2} was determined according to the effective frequency spectrum method[26] by using the observed heat capacities in the range 13–120 K and the infrared and Raman spectra. On the other hand, the normal heat capacity above T_{C2} was simply

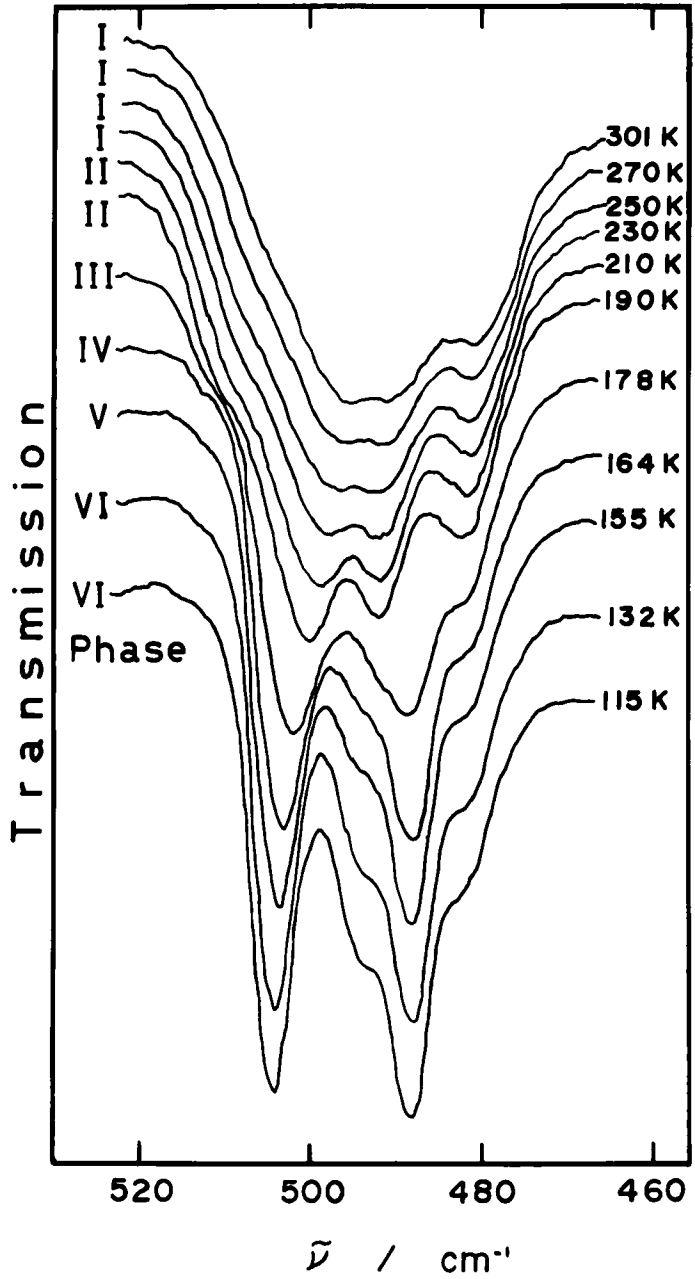

FIGURE 5 Infrared spectra of $Fe(C_5H_5)_2 \cdot 3(NH_2)_2CS$ in the range 520–460 cm^{-1} recorded for Nujol mulls.

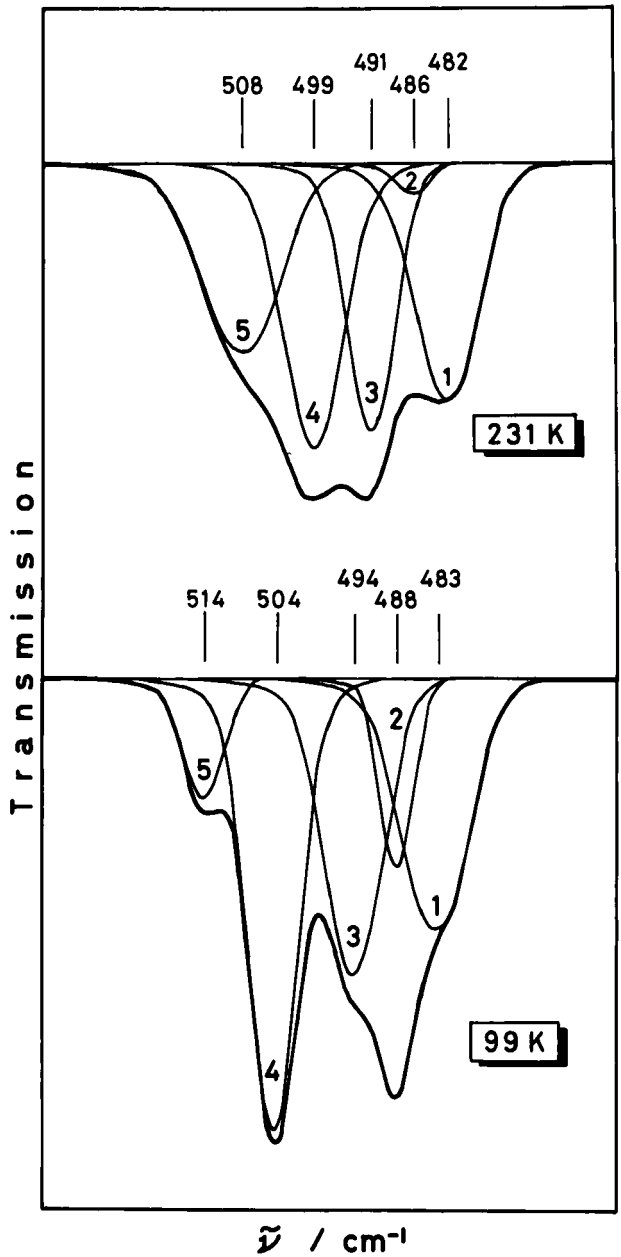

FIGURE 6 Resolution of the infrared spectra of $Fe(C_5H_5)_2 \cdot 3(NH_2)_2CS$ in the range 520–460 cm^{-1} into the constituent bands. The thick curve fits well to the observed spectrum recorded for KBr-disc. The assignment of each band is described in the text.

regarded as a curve which connects smoothly the heat capacities except for the phase transition regions. The normal heat capacities thus obtained are shown in Figure 1 by broken lines; a discontinuity of 7.48 J K^{-1} mol^{-1} occurred at T_{C2}.

The excess parts beyond the normal heat capacities are shown in Figure 7. Two phase transitions at T_{C1} and T_{C2} are closely correlated with each other. Although such a strong coupling does not seem to exist between the phase transitions at T_{C3} and T_{C4}, the tails of the excess heat capacities due to these transitions overlap in Phase III. The enthalpies and entropies associated with the phase transitions were determined by integrating the excess heat-capacity curve with respect to T and ln T, respectively. For these calculations, the results of the calorimetric enthalpy measurements across the respective phase transitions were also taken into account. Figure 8 illustrates the gain of the transition entropy with temperature. The first-order character of the phase transition at T_{C2} is clearly demonstrated. The numerical data concerning the thermodynamic quantities due to the phase transitions are summarized in Table III. The sum of the transition entropies amounted to 11.65 J K^{-1} mol^{-1}, most part of which was acquired at the two lowest-temperature phase transitions. The entropy change arising from the first-order contribution of the

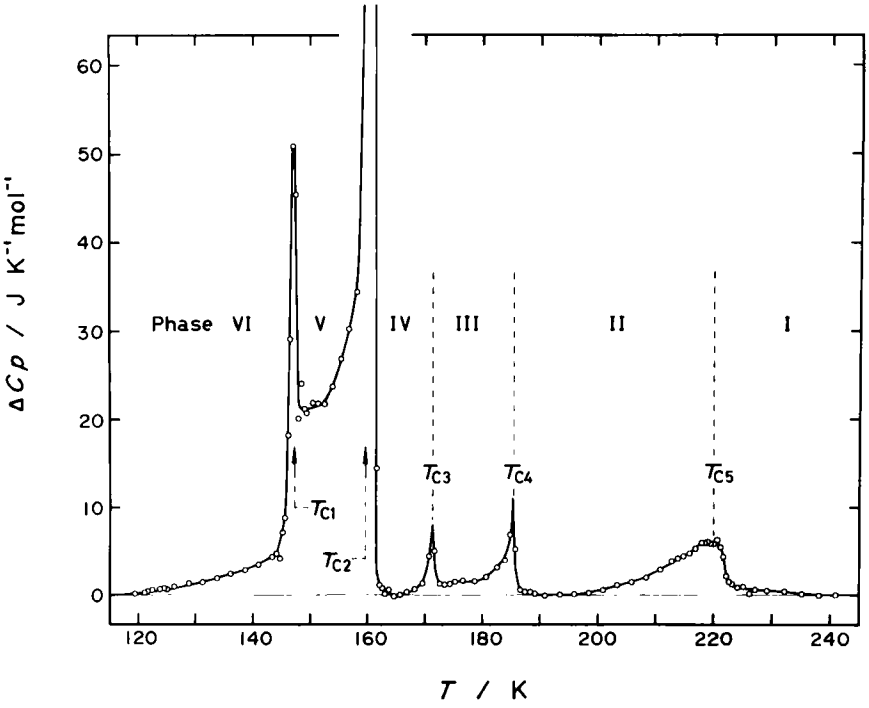

FIGURE 7 The excess heat capacities arising from the phase transitions of $Fe(C_5H_5)_2 \cdot 3(NH_2)_2CS$.

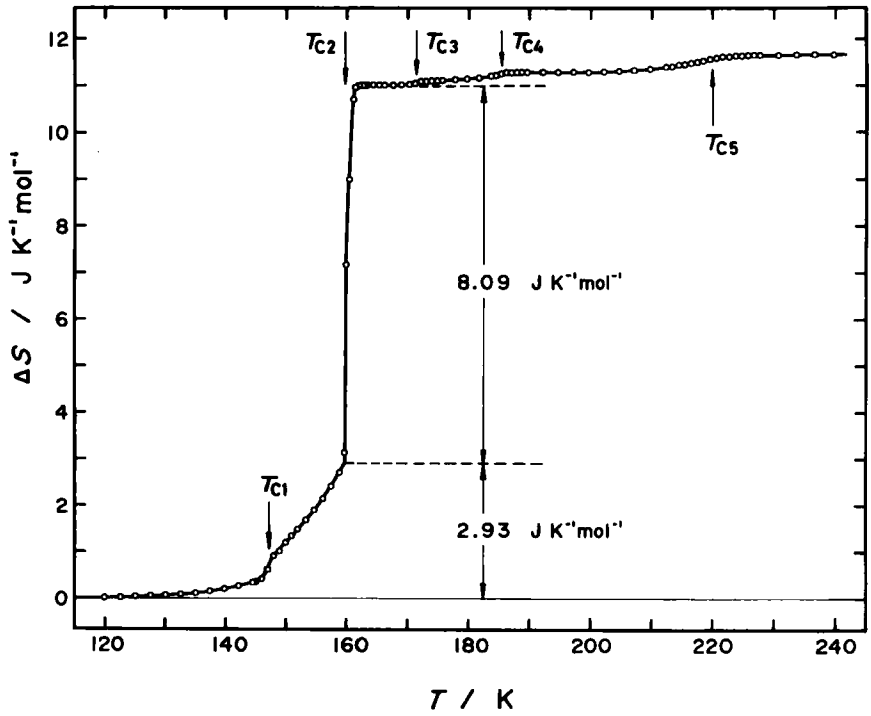

FIGURE 8 Gain of the transition entropy with temperature.

TABLE III

Thermodynamic quantities associated with the phase transitions of $Fe(C_5H_5)_2 \cdot 3(NH_2)_2CS$. The values in parentheses are the possible partitions into the respective phase transitions (*cf.* Section 5)

T_C / K	ΔH / kJ mol^{-1}		ΔS / J K^{-1} mol^{-1}	
147.2 (T_{C1})	(0.263)	1.737	(1.79)	11.02
159.79 (T_{C2})	(1.474)		(9.23)	
171.4 (T_{C3})	(0.014)	0.049	(0.08)	0.27
185.5 (T_{C4})	(0.035)		(0.19)	
220 (T_{C5})	0.077		0.36	
total	1.863		11.65	

transition at T_{C2} was 8.09 J K^{-1} mol^{-1} (see Figure 8). It is of interest to remark here that the total entropy change of 11.65 J K^{-1} mol^{-1} is very close to R ln 4 (= 11.53 J K^{-1} mol^{-1}); indicating the possible existence of four energetically nearly equal orientational sites for each ferrocene molecule in the thiourea channel lattice. This entropy value is intermediate between 5.31–5.5 J K^{-1} mol^{-1} due to the λ-type transition,[7,9,10] which occurs between the metastable phases of pure ferrocene crystal, and 17.13 J K^{-1} mol^{-1} of the phase transition,[7,9] which takes place between the stable phases of solid ferrocene. This fact suggests that, although the ferrocene molecules play dominant roles for all these transitions, the transition mechanism is quite different among these three.

5 MECHANISMS OF THE PHASE TRANSITIONS

When cyclic molecules are once included as the guest in the thiourea or urea host-lattices, the clathrate compound formed frequently exhibits multi-phase transition phenomena due to the guest molecules which are not observed for the pure crystal consisting solely of the respective guest molecules. Such examples are known for the thiourea-cycloalkanes[27-29] and the urea-trioxane adducts.[30]

Of the five phase transitions found for the present clathrate, the two lowest-temperature transitions at T_{C1} and T_{C2} are mainly concerned with the orientational order-disorder type mechanism of ferrocene molecules in the thiourea host-lattice, as the ^{57}Fe Mössbauer effect,[6] the X-ray diffraction analysis[4] and the proton magnetic resonance[31] show the onset of the reorientational motion around 162 K. According to Hough and Nicholson,[4] the structure of the clathrate consists of thiourea molecules which form a honeycomb of channels by spiralling with a pitch of 120° parallel to the c-axis. Within these channels, sites of point symmetry 32 are occupied by the ferrocene iron atoms (see Figure 9). In the high temperature phase above 162 K, the cyclopentadienyl rings of the ferrocene molecule are disordered and the time-averaged picture shows regions of three-dimensionally delocalized cyclopentadienyl electron density around the iron atoms. On the other hand, the five-fold axes of ferrocene molecules are frozen in a number of non-equivalent orientations at low temperatures.[31] Based on a detailed study of the ^{57}Fe Mössbauer effect, Gibb[6] has pointed out that the reorientational motion of ferrocene molecules is excited through two processes; one is the rapid reorientation about the channel axis of those molecules whose axes lie in the plane perpendicular to it (the α, β and γ-directions in Figure 9) and the other is the slow jump between those in the plane and the direction parallel to the channel axis (the z-direction in Figure 9). The activation energy for this jump has been found to be 15 kJ mol^{-1}.

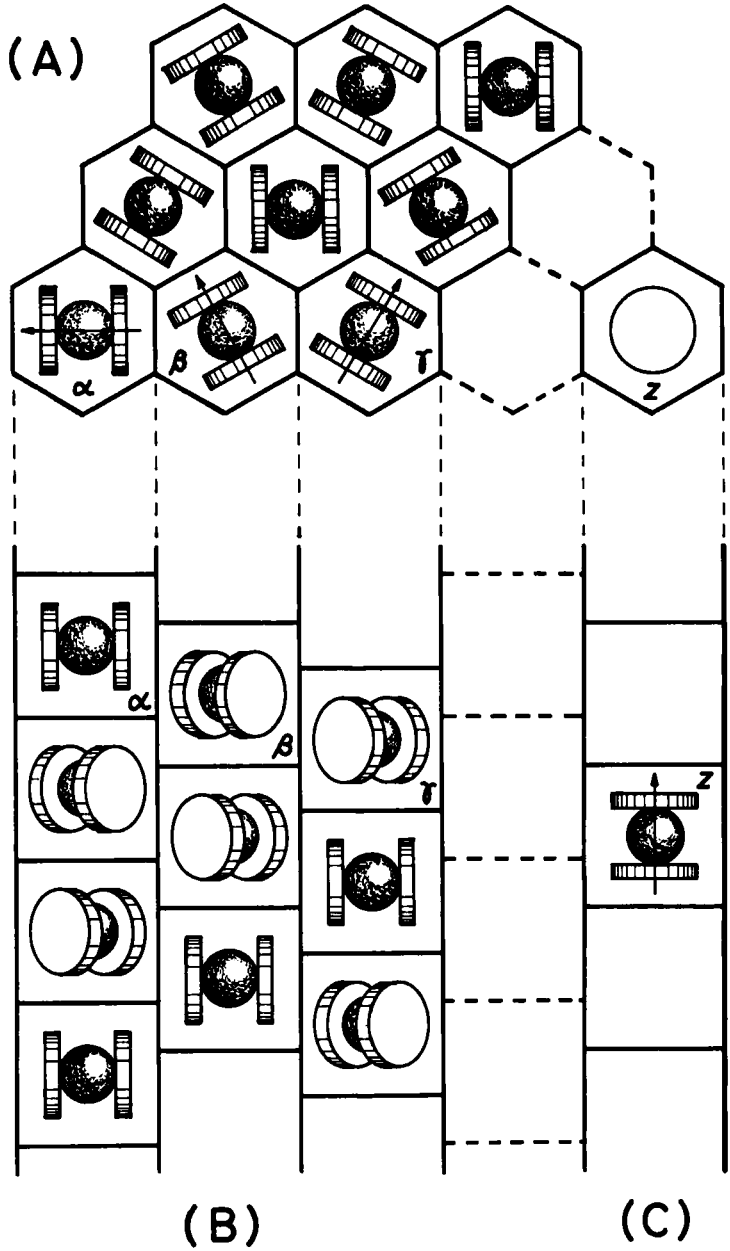

FIGURE 9 Schematic drawing showing the inclusion of ferrocene molecules in the honeycomb channels formed by the thiourea host-lattice. (A) and (B) are the top and side views of the suggested ordered phase. At high temperatures, ferrocene molecules are randomly oriented among the α, β, γ and z-directions.

The present calorimetric study revealed that the phase transition associated with the reorientational motion of the ferrocene molecules proceeds successively through two steps at T_{C1} and T_{C2}; supporting the two processes found by Gibb.[6] As described in Section 4, these two phase transitions are closely correlated with each other. We imagined that if the rotational disordering of ferrocene molecules would be realized in only one process, the tail of the excess heat capacity below T_{C2} might monotonically decrease without showing any anomaly. This hypothetical tail was estimated by fitting the excess heat capacity, ΔC_p, to an equation of the following form,

$$\Delta C_p = \frac{A}{T^2} \exp(-B/T). \tag{1}$$

As shown in the insert of Figure 10, four experimental points labelled by a, b, c and d lie on a straight line in the ln $(T^2 \Delta C_p)$ *versus* $1/T$ plot. The numerical constants determined by the least-squares method were

$$A = 4.302 \times 10^{12} \text{ J K mol}^{-1}$$

and

$$B = 2.440 \times 10^{3} \text{ K}. \tag{2}$$

The broken line in Figure 10 corresponds to the extrapolated values based on this equation. Since the extrapolated curve deviates from point-d at 153.93 K, it is reasonable to divide the transition enthalpy and entropy into the respective phase transitions at this temperature. The entropy again from 0 K to 153.93 K can be calculated by integrating Eq. (1) with respect to ln T:

$$\begin{aligned} \Delta S_{\text{calcd}}(\text{VI} \rightarrow \text{V}) &= \int_0^{153.93} \frac{A}{T^3} \exp(-B/T)\, dT \\ &= \left[\frac{A}{B} e^{-Bx}\left(x + \frac{1}{B}\right)\right]_{\infty}^{1/153.93} \\ &= 1.59 \text{ J K}^{-1} \text{ mol}^{-1}. \end{aligned} \tag{3}$$

On the other hand, the observed entropy change due to the transition from Phase VI to V, $\Delta S_{\text{obsd}}(\text{VI} \rightarrow \text{V})$, amounted to 1.79 J K^{-1} mol^{-1} in the same temperature range. This value is comparable with the entropy gained by the hypothetical tail given by Eq. (3). Therefore, the successive phase transitions can be interpreted in that the "pre-transitional part" of the main transition at T_{C2} was altered to a cooperative phase transition at T_{C1} (see Figure 10).

The total entropy of the transition at T_{C1} and T_{C2} was 11.02 J K^{-1} mol^{-1} and very close to R ln 4 (= 11.53 J K^{-1} mol^{-1}). If the rapid reorientations about the channel axis found by Gibb[6] would be fully excited before the slow jump process would begin, the entropy gain due to this disordering process would become R ln 3 (= 9.13 J K^{-1} mol^{-1}) as the possible orientations in the channel

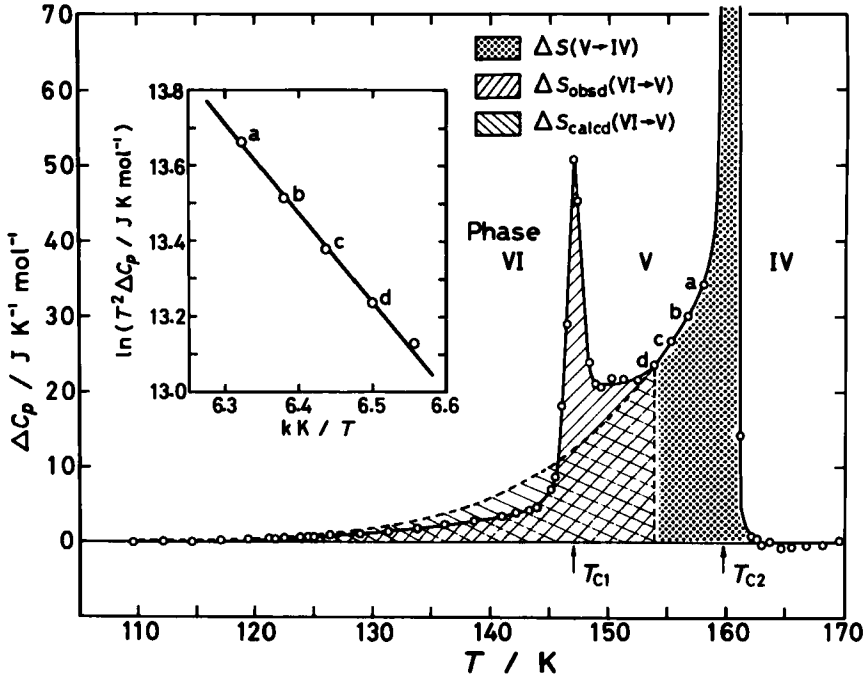

FIGURE 10 Separation of the closely correlated phase transitions at T_{C1} and T_{C2} into two parts.

plane are three (α, β and γ-directions in Figure 9). But this is not the case. As shown in Figure 8, the total entropy of 11.02 J K^{-1} mol^{-1} can be divided into the second-order contribution of 2.93 J K^{-1} mol^{-1} and the first-order component of 8.09 J K^{-1} mol^{-1}. If the former contribution would correspond to the so-called rapid process,[6] we should draw a physical picture in which the reorientational motion of a ferrocene molecule in the channel plane might not be independent from those of its neighboring ferrocene molecules but would be restricted by them. As the entropy due to the second-order component of 2.93 J K^{-1} mol^{-1} is well approximated by $\frac{1}{3}R \ln 3$ (= 3.04 J K^{-1} mol^{-1}), the reorientational motion in the channel plane would be excited in a unit of three ferrocene molecules. A possible unit, for example, consists of three adjacent ferrocene molecules located one-dimensionally along the channel axis in order of α, β and γ-directions. In this picture, the first-order component of the entropy involves the so-called slow jump process[6] as well as the disordering in the unit; *i.e.*, $\Delta S = R \ln 4 - \frac{1}{3}R \ln 3 = 8.48$ J K^{-1} mol^{-1}. This value coincides well with the observed entropy of 8.09 J K^{-1} mol^{-1}.

Finally discussed in this section are the origins of the remaining three phase transitions at T_{C3}(171.4 K), T_{C4}(185.5 K) and T_{C5}(220 K) with extremely small entropy changes; $\Delta S(T_{C5})$ was 0.36 J K^{-1} mol^{-1} while $\Delta S(T_{C3})$ and $\Delta S(T_{C4})$ were estimated to be 0.08 and 0.19 J K^{-1} mol^{-1} by assuming an appropriate

heat-capacity curve to separate these two phase transitions. A simple suspicion that anyone harbors for inclusion compounds like the present clathrate is a non-stoichiometry from a regular ratio of the guest to the host molecules. The orthorhombic thiourea crystal is known to exhibit three heat capacity anomalies associated with its ferroelectric character at 169.33, 171.20 and 200 K with the transition entropies of 0.17, 0.04 and 0.71 J K^{-1} mol^{-1}, respectively.[32] The temperature and the entropy of the transition at T_{C3} seem to bear a close resemblance to those of the two lowest-temperature phase transitions in solid thiourea. This correspondence, however, can be completely excluded for the following three reasons. (i) The present elementary and gravimetric analyses showed the correct molecular ratio of 3:1 for thiourea to ferrocene. (ii) The present dielectric constant measurements did not reveal any trace of the ferroelectric character. (iii) The transition entropies found for orthorhombic thiourea are too small to explain the entropy due to the transition at T_{C3} even though a small quantity of solid thiourea would be admixed in the specimen as the non-stoichiometry from the 3:1 inclusion compound.

On the other hand, pure ferrocene crystal exhibits the λ-type transition at 163.9 K with a secondary C_p maximum at 169 K between the metastable states.[7,9,10] The latter temperature is located rather near to T_{C3}. However, since this C_p maximum is closely correlated with the occurrence of the λ-type transition, a single appearance of the secondary C_p maximum in the present clathrate is quite implausible. Based on these considerations, the three phase transitions at T_{C3}, T_{C4} and T_{C5} can be concluded to be the intrinsic phenomena of the thiourea-ferrocene inclusion compound.

According to the X-ray diffraction analysis for pure ferrocene crystal by Calvarin and Berar,[33] the linear thermal expansion coefficients along the α_2 and α_3 principal axes show small anomalies around 180 and 220 K, which are respectively very close to T_{C4} and T_{C5}, as well as a dominant anomaly at the λ-point, although no heat capacity anomaly has been detected at these temperatures.[10] Hence the phase transitions at T_{C4} and T_{C5} may be interpreted as the intrinsic characters of the ferrocene molecule, which might be depressed in solid ferrocene, manifested in the inclusion compound in which ferrocene molecules are trapped in the potential cages formed by the thiourea host-lattice. We at first considered that a possible example of such intrinsic characters is a slight change in the electronic state of the ferrocene molecule because both solid ferrocene and the thiourea-ferrocene clathrate change their color from orange to yellow on cooling. In this case the metal-ring skeletal vibrational modes would shift their frequencies. However, as far as the present Raman and infrared spectroscopies are concerned, the $\nu_4(A_{1g})$ and $\nu_{16}(E_{1g})$ modes (Figure 3), the $\nu_{22}(E_{1u})$ mode (Figure 4), and the $\nu_{11}(A_{2u})$ and $\nu_{21}(E_{1u})$ modes (Figures 5 and 6) did not exhibit remarkable frequency shifts with temperature. Therefore, elucidation of the mechanisms of the phase transitions at T_{C4} and T_{C5} as well as that at T_{C3} should be deferred until more detailed molecular aspects will be accumulated.

6 CONCLUDING REMARKS

The present calorimetric study revealed that the reorientational excitation of the molecular axis of ferrocene proceeds in two steps accompanying the successive phase transitions at T_{C1} and T_{C2}. The first-stage excitation is realized by a group of ferrocene molecules as a unit keeping a phase relation concerning the direction of their molecular axes within the channel plane, while in the second-stage this restriction is lifted and the jump from the channel plane to the channel axis is allowed. However, we have not taken into account the reorientational motion of the cyclopentadienyl, C_5H_5, ring itself. Strictly speaking, we have tacitly assumed free rotation of the C_5H_5-ring over the whole phase transitions. This assumption does not conflict with the proton NMR of the thiourea-d_4-ferrocene clathrate[31]; the second moment of the absorption line in the range from 140 to 77 K, the lowest temperature of this experiment, has been well accounted for by a model that the five-fold axes of the ferrocene molecules are frozen in a number of non-equivalent orientations but reorientation of the C_5H_5-rings around the molecular five-fold axis is fully excited. Since the present heat-capacity data did not show any anomaly below 77 K, the slowdown of reorientational motion of the C_5H_5-rings can be concluded to proceed gradually without accompanying phase transition phenomenon at very low temperatures. In view of the fact[10] that the onset of this reorientational motion is responsible for the λ-type transition of solid ferrocene at 163.9 K, it is quite surprising that drastic reorientations concerning the molecular axes of ferrocene are fully excited in the thiourea-ferrocene inclusion compound in the temperature region even lower than the λ-point. At any rate, comparison of the mechanism responsible for the λ-type transition of solid ferrocene and that of the present clathrate clearly demonstrates that the molecular motion of ferrocene is definitely affected by the potential surroundings in which molecules are bounded.

One of the motivations for the present investigation was to elucidate the relationship between the unusual relaxation of the electric field gradient tensor of the ^{57}Fe Mössbauer spectroscopy[6] and the thermodynamic behavior reflected by it. Since the time scale of observation is quite different between the Mössbauer spectroscopy and the adiabatic calorimetry, the physical aspects to be observed are not necessarily identical. However, in the present case, these two methods played a complementary role to clarify the transition mechanism. In this regard, calorimetric study of (η-cyclohexatriene)(η-cyclopentadienyl)iron(II)hexafluorophosphate, $[Fe(C_5H_5)(C_6H_6)]PF_6$, seems to be instructive. Although this compound does not belong to a clathrate in the usual sense, Fitzsimmons *et al.*[34,35] observed a similar unusual relaxation in the ^{57}Fe Mössbauer effect arising from molecular reorientation of the cation within the ionic matrix formed by the anions which fulfills the role of the

channels of thiourea. In this case, one of the two C_5H_5-rings belonging to a ferrocene molecule is substituted with a C_6H_6-ring. Hence the cation has neither D_{5h} nor D_{5d} symmetry. A phase transition associated with reorientation of such an asymmetric moiety is of particular interest in comparison with the present result.

Hough and Nicholson[4] recorded the X-ray diffraction pattern of the thiourea-ferrocene clathrate at 100 K and suggested a change from rhombohedral with space group $R\bar{3}c$ to lower symmetry. However, detailed analyses have not been given. The knowledge of crystal structure is important for correct understanding of the phase transition. Precise X-ray diffraction analysis should, therefore, be performed not only for the lowest-temperature phase but also for Phases II, III, IV and V.

Acknowledgments

The authors express their sincere thanks to Dr. N. Oguni for permitting them to use the curve resolver, to Dr. T. Matsuo for his help in the dielectric constant measurements, to Messrs. S. Ishikawa, T. Yamamoto and M. Ohama for recording the infrared and Raman spectra.

References

1. S. M. M. Hagan, *Clathrate Inclusion Compounds* (Reinhold Pub. Corp., New York, 1962).
2. L. C. Fetterly, *Non-Stoichiometric Compounds* (edited by L. Mandelcorn, Academic Press, New York, 1964), Chap. 8, pp. 491–567.
3. R. Clement, R. Claude and C. Mazieres, *J. Chem. Soc. Chem. Commun.*, 654 (1974).
4. E. Hough and D. G. Nicholson, *J. Chem. Soc. Dalton*, 15 (1978).
5. H. V. Lenne, *Acta Cryst.*, **7**, 1 (1954).
6. T. C. Gibb, *J. Phys. C: Solid State Phys.*, **9**, 2627 (1976).
7. K. Ogasahara, M. Sorai and H. Suga, *Chem. Phys. Letters*, **68**, 457 (1979).
8. M. Sorai, S. Murakawa, K. Ogasahara and H. Suga, *Chem. Phys. Letters*, **76**, 510 (1980).
9. K. Ogasahara, M. Sorai and H. Suga, *Mol. Cryst. Liq. Cryst.*, **71**, 189–211 (1981).
10. J. W. Edwards, G. L. Kington and R. Mason, *Trans. Faraday Soc.*, **56**, 660 (1960).
11. J. W. Edwards and G. L. Kington, *Trans. Faraday Soc.*, **58**, 1334 (1962).
12. J. F. Berar, G. Calvarin, D. Weigel, K. Chhor and C. Pommier, *J. Chem. Phys.*, **73**, 438 (1980).
13. Y. Chatani and S. Nakatani, *Z. Krist.*, **144**, 175 (1976).
14. Y. Chatani, Y. Taki and H. Tadokoro, *Acta Cryst.*, **B33**, 309 (1977).
15. T. Matsuo, H. Suga and S. Seki, *J. Phys. Soc. Japan*, **30**, 785 (1971).
16. T. Matsuo, *J. Phys. Soc. Japan*, **30**, 794 (1971).
17. M. Yoshikawa, M. Sorai, H. Suga and S. Seki, to be published.
18. T. Matsuo and H. Suga, *Solid State Commun.*, **21**, 923 (1977).
19. A. L. Solomon, *Phys. Rev.*, **104**, 1191 (1956).
20. G. J. Goldsmith and J. G. White, *J. Chem. Phys.*, **31**, 1175 (1959).
21. E. R. Lippincott and R. D. Nelson, *Spectrochim. Acta*, **10**, 307 (1958).
22. J. E. Stewart, *J. Chem. Phys.*, **26**, 248 (1957).
23. H. Takahashi, B. Schrader, W. Meier and K. Gottlieb, *J. Chem. Phys.*, **47**, 3842 (1967).
24. A. Bandy, G. L. Cessac and E. R. Lippincott, *Spectrochim. Acta*, **28A**, 1807 (1972).
25. I. J. Hyams, *Spectrochim. Acta*, **29A**, 839 (1973).
26. M. Sorai and S. Seki, *J. Phys. Soc. Japan*, **32**, 382 (1972).
27. R. Clement, M. Gourdji and L. Guibe, *Mol. Phys.*, **21**, 247 (1971).

28. A. F. G. Cope, D. J. Gannon and N. G. Parsonage, *J. Chem. Thermodyn.*, **4**, 829 (1972).
29. R. Clement, C. Mazieres, M. Gourdji and L. Guibe, *J. Chem. Phys.*, **67**, 5381 (1977).
30. R. Claude, R. Clement and A. Dworkin, *J. Chem. Thermodyn.*, **9**, 1199 (1977).
31. R. Clement, M. Gourdji and L. Guibe ,*Chem. Phys. Letters*, **72**, 466 (1980).
32. E. Chang and E. F. Westrum, Jr., unpublished data cited in *Physics and Chemistry of the Organic Solid State*, Vol. 1 (edited by D. Fox, M. M. Labes and A. Weissberger, Interscience, New York, 1963), Chap. 1.
33. G. Calvarin and J. F. Berar, *J. Appl. Cryst.*, **8**, 380 (1975).
34. B. W. Fitzsimmons, *J. Phys.* (*Paris*), **41**, C1-33 (1980).
35. B. W. Fitzsimmons and A. R. Hume, *J. Chem. Soc. Dalton*, 180 (1980).